Chemical Science

ROYAL SOCIETY OF CHEMISTRY

EDGE ARTICLE

View Article Online
View Journal

Cite this: DOI: 10.1039/d6sc00859c

All publication charges for this article have been paid for by the Royal Society of Chemistry

Revealing transport kinetics for efficient electrochemical conversion of captured CO_2 in amine solutions

Zhihui Lv, [a] Kang Liu, [b] Chun-Qing Yin, [a] Lin Du, [a] Min Liu *[bc] and Xin-Ming Hu *[ad]

Received 31st January 2026
Accepted 29th April 2026

DOI: 10.1039/d6sc00859c

rsc.li/chemical-science

Direct electrochemical conversion of captured CO_2 in amine solutions offers a promising route to upgrade dilute CO_2 into valuable chemicals, bypassing the energy-intensive stripping step. However, this reaction is obscured by the complex equilibrium among carbamate, bicarbonate, dissolved CO_2, and protonated ammonium in CO_2-loaded amine solutions and suffers from low selectivity due to the competing reduction of protonated ammonium. Here, we elucidate the reaction mechanism and reveal the mass transport as the governing factor for electrochemical conversion of captured CO_2 in monoethanolamine (MEA), diethanolamine (DEA), and triethanolamine (TEA), which are the representatives of primary, secondary, and tertiary amines with the same functionality. Bicarbonate-derived CO_2, rather than carbamate, is identified as the reactive species for CO generation across all amines. TEA is found to be the optimal amine, offering the highest CO selectivity (80%) and stability with heterogenized cobalt phthalocyanine as the catalyst. This is attributed to the significantly hindered mass transport of both reactive bicarbonate and protonated ammonium in TEA than in the other two amines, with protonated TEA exhibiting particularly sluggish diffusion. These findings pave the way for the rational design of amine systems for efficiently converting captured CO_2 through mass transport manipulation.

Introduction

Excessive CO_2 emission causes global climate change, posing severe threats to ecosystems and human health.[1,2] Electrochemical CO_2 conversion has emerged as a promising solution to mitigate the CO_2 accumulation and produce valuable fuels and chemicals (*e.g.*, CO, $HCOO^-$, C_2H_4, and C_2H_5OH).[3–6] This approach offers distinct advantages, such as tuneable product selectivity, mild operating conditions, and high compatibility with renewable electricity.[7] Among the possible products, CO has attracted considerable attention because of its role as a key feedstock for Fischer–Tropsch synthesis.[8] Considerable progress has been made with state-of-the-art catalysts, such as Au/Ag nanostructures,[9,10] supported metal complexes,[11–14] and single atom catalysts (SACs),[15–18] which have achieved high faradaic efficiencies and industrial-level current densities for CO_2-to-CO conversion.

Despite these advances, two major challenges limit the practical applications of electrochemical CO_2 conversion. First, conventional electrochemical systems rely on high-purity, pressurized CO_2 gas, which comes from energy-intensive CO_2 capture, desorption, purification, and compression processes (Fig. 1a).[19,20] Second, the overall CO_2 utilization efficiency remains low in the gas-fed systems, typically <20% for CO_2-to-CO conversion,[21,22] due to CO_2 loss through carbonate formation or incomplete reaction, which further requires costly product separation and CO_2 recycling.[23]

To overcome these barriers, direct electrochemical conversion of captured CO_2 has recently gained traction as a strategy that integrates carbon conversion with capture (Fig. 1b). By electrolyzing CO_2-loaded capture media (*e.g.*, bicarbonate or CO_2-amine adducts), this strategy circumvents the need for CO_2 release and purification, while simultaneously improving carbon utilization.[24–30] Li *et al.* performed an energy comparison between sequential and integrated CO_2 capture and electrochemical conversion.[25] They estimated that if the electrolyzer for captured CO_2 electrolysis performs comparably to the conventional CO_2-fed system, the direct conversion could save nearly 44% in energy consumption relative to the conventional sequential process.

Among various capture media, amine solutions dominate industrial CO_2 capture due to their high absorption capacity, rapid kinetics, and low cost.[31,32] Accordingly, direct

[a]Environment Research Institute, Shandong University, Qingdao 266237, China. E-mail: huxm@sdu.edu.cn

[b]Hunan Joint International Research Center for Carbon Dioxide Resource Utilization, State Key Laboratory of Powder Metallurgy, School of Physics, Central South University, Changsha 410083, China. E-mail: minliu@csu.edu.cn

[c]School of Metallurgy and Environment, Central South University, Changsha 410083, China

[d]Shandong Key Laboratory of Environmental Processes and Health, Shandong University, Qingdao 266237, China

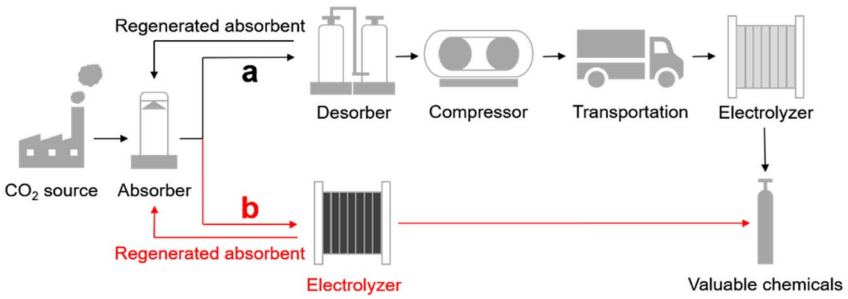

Fig. 1 (a) Conventional and (b) integrated systems for CO_2 capture and electrochemical conversion.

electrochemical conversion of captured CO_2 in amines into CO presents a compelling route to obtain value-added chemicals and regenerate the amine absorbents. Notably, Sargent and co-workers first demonstrated the electrochemical conversion of CO_2-loaded monoethanolamine (MEA), achieving an optimal faradaic efficiency of 72% for CO production at -50 mA cm^{-2} using Ag catalysts in a flow cell.[33] However, Gallant and co-workers reported only ~20% CO faradaic efficiency in an H-cell with the same catalyst and MEA medium,[34] while Kim *et al.* achieved a CO selectivity of 65% at a comparable current density using a nickel single-atom catalyst in a membrane electrode assembly.[35]

More recently, Li *et al.* identified piperazine (PZ) as an optimal capture medium for integrated CO_2 capture and conversion, which showed superior reaction kinetics to MEA, due to the formation of the charge-neutral H^+PZCOO^- intermediate in CO_2-loaded PZ solution.[36] In their study, an optimal selectivity of 38% for CO production was reported when electrolyzing the CO_2-loaded PZ solution at 10 mA cm^{-2} at room temperature with a nickel single-atom catalyst, while the selectivity could be increased to 75% at an elevated electrolysis temperature (60 °C).

These previous studies indicate two key points. First, the direct electrochemical conversion of captured CO_2 in amine solutions is feasible but suffers from low efficiency (*i.e.*, poor selectivity), due to the competing hydrogen evolution reaction (HER) arising from the reduction of protonated ammoniums in the solution. Second, the amine structure strongly influences the conversion efficiency of captured CO_2, yet an in-depth evaluation across varying amines is still lacking.

In addition, the identity of the true reactant in CO_2-loaded amine solutions remains contentious. Some researchers proposed carbamate (CO_2-amine adduct) as the active species for CO generation,[33,36] while others attributed CO production to dissolved or liberated CO_2 coming from carbamate dissociation.[34,35] The poor understanding of the reaction process of captured CO_2 in amine solutions poses challenges for rational system design to optimize the conversion efficiency. Therefore, exploring an optimal amine and elucidating the reaction mechanism are imperative for achieving selective conversion of captured CO_2 in amine solutions.

In this work, we show that the tertiary amine (triethanolamine, TEA) outperforms the primary (MEA) and secondary (diethanolamine, DEA) amines in the direct electrochemical conversion of captured CO_2 solutions using cobalt phthalocyanine supported on carbon black (CoPc/CB) as a model catalyst. Across all amines, CO emerges as the dominant product, with the selectivity and stability following MEA < DEA < TEA. Comprehensive analysis combining ^{13}C nuclear magnetic resonance (NMR), *in situ* infrared spectroscopy, density functional theory (DFT), determination of diffusion coefficients, and deuterated water experiments reveals a new reaction pathway for the conversion of captured CO_2, that is, dissociated CO_2 from bicarbonate, rather than carbamate, is electrochemically reduced to form CO, irrespective of amine types. Moreover, mass transport is identified as the governing factor in determining the conversion efficiency of captured CO_2. The smallest diffusion coefficient in TEA hinders the transport of both reactive bicarbonate and protonated ammonium, suppressing hydrogen evolution more significantly, thereby enhancing CO selectivity and operational stability. As a result, a maximum selectivity of 80% for CO production can be achieved in the electrolysis of CO_2-loaded TEA, superior to MEA, DEA, and many reported amine systems. These insights establish mass transport as a critical determinant in direct conversion of captured CO_2 in amine solutions and provide guidelines for rational amine selection and system optimization.

Experimental

Chemicals

All reagents used in this work were obtained from commercial suppliers without further purification. Cobalt phthalocyanine (CoPc) and deuterium oxide (D_2O) were purchased from J&K Scientific Co., Ltd Carbon black (CB, cabot vulcan XC-72) was purchased from Macklin Biochemical Co., Ltd *N*,*N*-dimethylformamide (DMF), ethanol, isopropanol, potassium bicarbonate ($KHCO_3$), and hydrochloric acid (HCl) were purchased from Sinopharm Chemical Reagent Co., Ltd Nafion solution (5 wt%) and silver nanopowder were from Sigma-Aldrich Chemical Reagent Co. Ltd Nickel chloride hexahydrate ($NiCl_2 \cdot 6H_2O$), melamine, monoethanolamine (MEA), diethanolamine (DEA), triethanolamine (TEA), and hydroxymethylferrocene were purchased from Shanghai Aladdin Bio-Chem Technology Co. Ltd Potassium chloride (KCl) and lithium chloride (LiCl) were obtained from Shanghai Maclin Biochemical Technology Co. Ltd The PET plastic waste used to

synthesize the nickel single-atom catalyst (Ni–N–C) came from used water bottles. Ultrapure water (18.2 MΩ cm) from a Milli-Q system was used in all experiments.

Catalyst synthesis

The CoPc/CB catalyst was prepared according to reported procedures.[37] First, 6 mg of CoPc was dissolved in 300 mL DMF. Subsequently, 600 mg of CB was added into the above solution and sonicated for 30 min. The resulting suspension was stirred for 24 h at room temperature and filtered. Finally, the CoPc/CB catalyst was obtained after washing with DMF, ultrapure water, and ethanol, and dried *in vacuo* at 60 °C overnight.

The Ni–N–C catalyst was prepared according to the literature.[38] First, 1.0 g $NiCl_2 \cdot 6H_2O$, 2.0 g melamine, 5.5 g KCl, and 4.5 g LiCl were ground in a mortar. Next, 2.0 g PET plastic waste was cut into small pieces (*ca.* 0.5 × 0.5 cm^2) and added into the mixture. Then, the resulting mixture was transferred into a quartz boat and pyrolyzed in a tube furnace at 800 °C for 2 h under an Ar flow. After cooling down to room temperature, the product was washed with 1 M HCl at 60 °C for 4 h, followed by washing with ultrapure water and methanol. Afterwards, the product was dried overnight at 60 °C *in vacuo*. Finally, the Ni–N–C catalyst was obtained after a secondary carbonization under the same pyrolysis conditions as the first time.

Electrochemical measurements

The preparation of the working electrodes was as follows. The catalyst ink was prepared by dispersing the CoPc/CB, Ni–N–C, or Ag nanopowder catalyst (6 mg) in a mixture of isopropanol (90 μL), Nafion solution (60 μL), and ultrapure water (450 μL) under sonication for 30 min. Subsequently, 100 μL of the catalyst ink was drop cast onto both sides of the hydrophobic carbon paper (TGP-H-060, 20% PTFE) and dried in air. The effective area of the working electrode was 2 cm^2, and the catalyst loading was 0.5 mg cm^{-2}. Controlled potential electrolysis was conducted on an electrochemical station (CHI 760E) in a three-electrode H-cell. The carbon paper coated with the catalyst was used as the working electrode, and Ag/AgCl and platinum mesh were used as the reference electrode and counter electrode, respectively. The anolyte was 0.5 M $KHCO_3$ (30 mL), while the catholyte was CO_2-loaded MEA, DEA, and TEA solutions (saturated with CO_2 gas before use, 30 mL), respectively. The pH values of the catholytes were measured with a Mettler Toledo pH meter and are listed in Table S1. A Nafion 117 membrane was used to separate the cathodic and anodic chambers.

Prior to the test, the catholytes were purged with Ar (50 sccm) for 15 min to remove dissolved CO_2, and the working electrodes were activated by applying a potential (−0.55 V *vs.* RHE) for 5 min. The electrolysis was carried out at controlled potentials under an Ar (10 sccm) atmosphere with electrolyte stirring. The potential against Ag/AgCl was converted to the potential against the reversible hydrogen electrode (RHE) according to eqn (1):

$$E(\mathrm{RHE}) = E(\mathrm{Ag/AgCl}) + 0.197 + \frac{RT}{F} \times \ln 10 \times \mathrm{pH} \quad (1)$$

where R is the ideal gas constant, 8.314 J mol^{-1} K^{-1}; T is room temperature (K); F is the Faraday constant, 96 485 C mol^{-1}; the pH value is for Ar-purged CO_2-loaded 2 M amine solutions.

The gas outlet in the cathodic chamber was connected to the inlet of the gas chromatograph (Fuli GC9790II), where the gaseous products were analysed online. The cathodic electrolyte was analysed by using a nuclear magnetic resonance (NMR) spectrometer. The faradaic efficiency (FE) of CO and H_2 was calculated according to eqn (2):

$$\mathrm{FE} = \frac{n \times C \times v \times F \times P}{I \times R \times T} \times 100\% \quad (2)$$

where n is the number of electrons transferred to CO or H_2; C is the concentration of CO or H_2 in the outlet gas stream; v is the rate of outlet gas flow; F is the Faraday constant, 96 485 C mol^{-1}; P is the atmospheric pressure, 101 325 Pa; I is the current recorded at the sampling time; R is the ideal gas constant, 8.314 J mol^{-1} K^{-1}; T is room temperature (K).

To determine the diffusion coefficient of the CO_2-loaded amine solutions, cyclic voltammetry experiments were conducted on an electrochemical station (CHI 760E) in an H-cell. A glassy carbon disc electrode (diameter = 3 mm), Ag/AgCl electrode, and platinum mesh were used as the working electrode, reference electrode, and counter electrode, respectively. The anolyte was 0.5 M $KHCO_3$, while the catholyte was CO_2-loaded 2 M amine solutions, 2 M ammonium chloride solutions of the corresponding amines, or 2 M potassium bicarbonate solution. 2 mM hydroxymethylferrocene was added into the catholyte as the redox couple. The cyclic voltammograms were recorded at scan rates of 50, 100, 200, 500, 1000, 2000, 5000, and 100 000 mV s^{-1} in a random order. The diffusion coefficient was calculated according to eqn (3):[39]

$$i_p = 0.446 mFAC^0 \left(\frac{mFv'D_0}{RT}\right)^{\frac{1}{2}} \quad (3)$$

where i_p is the peak current for oxidation of hydroxymethylferrocene measured by cyclic voltammetry; m is the number of electrons transferred for oxidation of hydroxymethylferrocene; F is the Faraday constant, 96 485 C mol^{-1}; A is the surface area of the glassy carbon disc electrode; C^0 is the concentration of hydroxymethylferrocene; v' is the scan rate; D_0 is the diffusion coefficient; R is the ideal gas constant, 8.314 J mol^{-1} K^{-1}; T is room temperature (K).

In situ ATR-FTIR

In situ attenuated total reflection-Fourier transform infrared (ATR-FTIR) spectra were recorded on a Bruker INVENIO spectrometer with a MCT detector. Ag/AgCl and a platinum wire served as the reference electrode and counter electrode, respectively. The working electrode was prepared by depositing the same CoPc/CB catalyst ink onto a silicon prism plated with a gold layer. The electrolyte was Ar-degassed CO_2-loaded 2 M MEA or TEA solution. IR spectra were recorded during electrolysis at potentials from 0.05 V to −1.05 V *vs.* RHE in 0.1 V intervals under continuous Ar purging. Each spectrum was acquired over 100 scans at a resolution of 4 cm^{-1}. The

background spectrum was recorded at 0.05 V *vs.* RHE for baseline subtraction.

DFT calculations

The density functional theory (DFT) calculations were performed by using the Vienna *ab initio* simulation package (VASP).[40,41] The projector augmented wave (PAW) method was adopted to deal with the electron–ion interactions.[42] The generalized gradient approximation (GGA) of Perdew–Burke–Ernzerhof (PBE) was used to treat the electron–electron exchange and correlation functional.[43,44] The cutoff energy was set to 400 eV. The calculations were performed with a convergence criterion of 0.02 eV $Å^{-1}$ in forces and 1×10^{-4} eV $atom^{-1}$ in energy. Van der Waals (VDW) forces were corrected with the D2 method of Grimme.[45] We used the implicit solvent model of VASPsol to deal with solvent effects in our calculations.[46,47] The Debye length was set to 3 Å to simulate the experimental acid conditions (1 M). The dielectric constant for water was set to a relative permittivity value of 80.

We constructed a 9 × 5 graphene rectangular supercell slab containing 180 carbon atoms. Cobalt phthalocyanine was supported on the slab (Fig. S1). In addition, we constructed a network structure consisting of two MEA molecules, six water molecules, and one CO_2 molecule to simulate the interactions between molecules. The total number of atoms in the system is 280 atoms. The vacuum layer was set at 18 Å to simulate a realistic surface system and eliminate the influence of periodicity on the system. Only Gamma *k*-point was used for the *k*-space integration. We explore the mechanism of CO_2 conversion by evaluating the reaction energy of the system.

Results and discussion

Electrolysis of CO_2-loaded amine solutions

To investigate the effect of amine structures, we conduct electrolysis of captured CO_2 in three different types of amine solutions, including MEA, DEA, and TEA, which are the representatives of primary, secondary, and tertiary amines, respectively (Fig. 2a). The selection of these three amines is because they have the same hydroxyethyl functional group (*i.e.*, $–CH_2CH_2OH$) and vary only in the number of such a group (*i.e.*, one hydroxyethyl for MEA, two for DEA, and three for TEA). This can avoid complications arising from different functional groups.

The electrolysis of CO_2-loaded amine solutions is investigated in an H-cell using CoPc/CB as the catalyst, which is prepared according to reported procedures.[37] Prior to electrolysis, the CO_2-loaded amine solutions are purged with Ar to remove dissolved CO_2. The electrolysis under an Ar atmosphere produces CO and H_2 as the only products, and no product is detected in the electrolyte solutions (Fig. 2, S2 and S3). This suggests that the captured CO_2 in all examined amine solutions can be converted to the CO product by electrocatalysis, since no external CO_2 is supplied.

The results for electrolysis of captured CO_2 in different concentrations of MEA solutions (*i.e.*, 1, 2, and 5 M) are shown in Fig. S3. The electrolysis in CO_2-loaded 2 and 5 M MEA exhibits similar partial current densities for CO production ($|j_{CO}|$), which are both significantly higher than $|j_{CO}|$ recorded in 1 M MEA at the same potentials. Moreover, the partial current density for H_2 generation ($|j_{H_2}|$) in 5 M MEA is the lowest among the three concentrations. Accordingly, the faradaic efficiency for CO production (FE_{CO}) recorded in the three MEA solutions generally follows an order of 1 M < 2 M < 5 M, while the faradaic efficiency for H_2 evolution (FE_{H_2}) follows the opposite order. It should be noted that both $|j_{CO}|$ and FE_{CO} recorded in 2 M MEA are significantly higher than those in 1 M MEA, which is attributed to the higher concentration of captured CO_2 in the former solution. However, the differences in $|j_{CO}|$ and FE_{CO} between 2 M and 5 M MEA are very small, showing that further increasing the amine concentration does not enhance the conversion of captured CO_2. Notably, CO_2-loaded 5 M DEA and TEA solutions are too viscous to carry out the electrolysis. Therefore, 2 M amine solutions are optimal for electrochemical conversion and used for subsequent experiments.

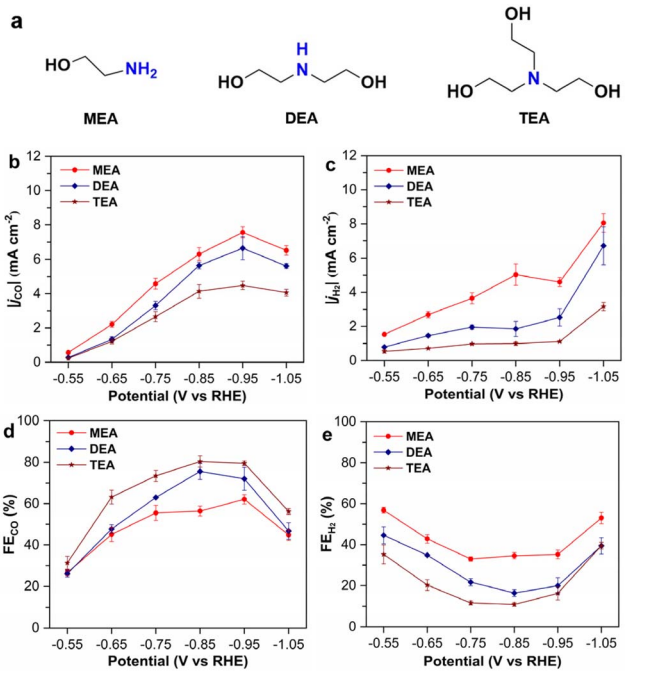

Fig. 2 (a) The structures of MEA, DEA, and TEA. (b) $|j_{CO}|$, (c) $|j_{H_2}|$, (d) FE_{CO}, and (e) FE_{H_2} recorded for the electrolysis of captured CO_2 in 2 M MEA, DEA, and TEA solutions using the CoPc/CB catalyst.

Among different amine solutions, the highest current density ($|j|$), $|j_{CO}|$, and $|j_{H_2}|$ are all observed in CO_2-loaded MEA solution across the same electrolysis potentials, following a sequence of MEA > DEA > TEA (Fig. 2b, c and S4a). This reveals the highest activity for both CO production and the HER in CO_2-loaded MEA solution. As for the selectivity, FE_{H_2} recorded in different CO_2-loaded amine solutions still follows the same order of MEA > DEA > TEA; however, FE_{CO} follows the opposite order of MEA < DEA < TEA (Fig. 2d and e). This points to the fact that the highest selectivity toward CO production for the electrochemical conversion of captured CO_2 is achieved in TEA

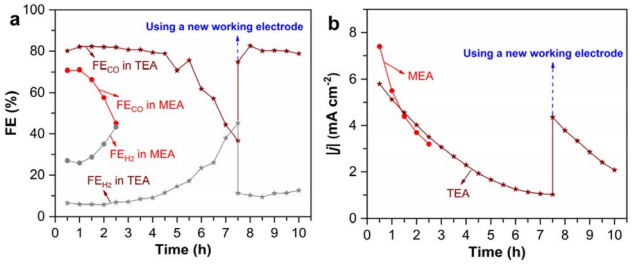

Fig. 3 (a) FE_{CO}, FE_{H_2}, and (b) $|j|$ recorded for the prolonged electrolysis of captured CO_2 in 2 M MEA and TEA solutions at −0.85 V *vs.* RHE using the CoPc/CB catalyst. After electrolysis for 7.5 h in TEA, a new working electrode is used to continue the electrolysis.

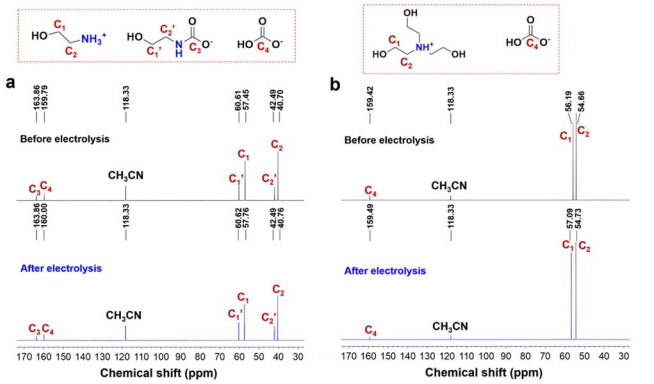

Fig. 4 ^{13}C NMR spectra before and after prolonged electrolysis of captured CO_2 in 2 M (a) MEA and (b) TEA solutions at −0.85 V *vs.* RHE using the CoPc/CB catalyst until the FE_{CO} is lower than 50%.

among the three types of amines. Specifically, the maximum FE_{CO} up to 80% is recorded for the electrolysis of captured CO_2 in 2 M TEA, higher than that in DEA (76%), MEA (69%), and other amine systems reported in the literature (Table S2).[33–35,48] Although the current density recorded in TEA is lower than in MEA and DEA using CoPc/CB, it is substantially higher than those reported for other amine systems using different catalysts under similar potentials.

Given that the conversion efficiency of captured CO_2 in DEA is intermediate between that in MEA and in TEA, additional efforts are directed to studying the electrochemical conversion of captured CO_2 in the latter two amines. The electrolysis of CO_2-loaded 2 M MEA and TEA is conducted for a prolonged period to study the stability of the two different systems. In 2 M MEA, FE_{CO} declines rapidly to below 50% within 2.5 h, accompanied by a rapid increase in FE_{H_2} (Fig. 3a). In comparison, FE_{CO} in TEA remains approximately 80% for the first 4.5 h of electrolysis and drops below 50% at 7 h under the same electrolysis conditions. Similarly, the $|j|$ in MEA also decreases much faster than in TEA (Fig. 3b). These results suggest that the electrolysis stability in CO_2-loaded 2 M TEA is much higher than in MEA under identical conditions, although the overall stability in TEA necessitates further optimization.

To understand the reason for decreasing efficiency over electrolysis time, we replace the CoPc/CB working electrode with a fresh one after 7.5 h of electrolysis in 2 M TEA. Encouragingly, both FE_{CO} and FE_{H_2} return to their original levels, and $|j|$ also recovers substantially (Fig. 3). This reveals that the decreased efficiency for the electrolysis of CO_2-loaded amine solutions is mainly due to the deactivation of the CoPc/CB catalyst, rather than the consumption of captured CO_2 in the amine solution. The catalyst deactivation probably originates from the HER, which can induce hydrogenation of the phthalocyanine structure.[49] Notably, the HER is greatly inhibited in TEA solution, which results in enhanced selectivity and stability for CO production.

Identification of reactive species

To uncover the underlying reason of divergent conversion efficiencies, we first investigate the chemical speciation of captured CO_2 in different amine solutions. MEA, as a primary amine, captures CO_2 through the formation of carbamate ($RNHCOO^-$, R═$HOCH_2CH_2$) together with protonated ammonium (MEA-H^+) as the primary products (eqn (4)). This is confirmed by the ^{13}C NMR spectrum of CO_2-loaded MEA solution, where a peak at a chemical shift of 163.86 ppm assigned to $RNHCOO^-$ is clearly observed (Fig. 4a).[50,51] The formation of MEA-H^+ is shown by the presence of two peaks at chemical shifts of 57.45 and 40.70 ppm, corresponding to the carbon atoms (C_1 and C_2) adjacent to the ammonium group. A distinct peak at 159.79 ppm is also observed, which is attributed to bicarbonate (HCO_3^-).[50,51] Notably, the peak for HCO_3^- is more intense than $RNHCOO^-$, which shows that a substantial portion of $RNHCOO^-$ undergoes hydrolysis to form HCO_3^- (eqn (5)).

$$2RNH_2 + CO_2 \rightleftharpoons RNHCOO^- + RNH_3^+ \quad (4)$$

$$RNHCOO^- + H_2O \rightleftharpoons HCO_3^- + RNH_2 \quad (5)$$

$$R_3N + CO_2 + H_2O \rightleftharpoons R_3NH^+ + HCO_3^- \quad (6)$$

TEA, as a tertiary amine, captures CO_2 through the formation of HCO_3^- and also a protonated ammonium (TEA-H^+, eqn (6)).[51] This is confirmed by the ^{13}C NMR spectrum of CO_2-loaded TEA solution, where a peak with a chemical shift of 159.42 ppm assigned to HCO_3^- is clearly observed (Fig. 4b). The formation of TEA-H^+ is shown by the presence of two peaks at chemical shifts of 56.19 and 54.66 ppm, corresponding to the carbon atoms (C_1 and C_2) adjacent to the ammonium group.

In addition, we observe comparable concentrations of CO_2 in the headspace (C_{CO_2}) of the electrolysis system across the three CO_2-loaded amine solutions by gas chromatography (Fig. S4b). This observation suggests the *in situ* generation of CO_2 from the dissociation of carbamate and/or bicarbonate ions. It also reveals that the amount of CO_2 consumed during the short-term electrolysis (15 min) is negligible compared to the amount of captured CO_2 in various amine solutions.

The analysis shows that the CO_2-loaded amine solutions contain a complex mixture of chemical species. The carbon source for CO production could be carbamate, bicarbonate, or free CO_2, while the proton source for hydrogen evolution could

be water, bicarbonate, or ammonium. Therefore, identifying the actual reactants involved in the electrolysis is crucial to understand the divergent conversion efficiencies of captured CO_2 in different amine solutions. To unveil the reactant for CO production, we recorded the ^{13}C NMR spectra of the electrolyzed CO_2-loaded amine solutions and compared it with those before electrolysis (Fig. 4). In the CO_2-loaded 2 M MEA solution, the intensity for the chemical shift of $RNHCOO^-$ is almost unchanged, while the intensity for HCO_3^- decreases after electrolysis at −0.85 V *vs.* RHE. This suggests that HCO_3^-, instead of $RNHCOO^-$, is consumed and converted to the CO product. In the CO_2-loaded 2 M TEA solution, HCO_3^- is also consumed after electrolysis at −0.85 V *vs.* RHE. These results demonstrate that the CO product originates from HCO_3^- in both CO_2-loaded MEA and TEA solutions, while $RNHCOO^-$ cannot be directly reduced to CO.

In situ attenuated total reflection-Fourier transform infrared (ATR-FTIR) spectroscopy is employed to get more insights into the reaction species for the conversion of captured CO_2 in MEA and TEA solutions. We first record the *in situ* ATR-FTIR spectra during the process of CO_2 capture in 2 M MEA and TEA solutions. When CO_2 is continuously introduced into the MEA solution, a series of positive peaks appear in the spectra and progressively intensify with time evolution (Fig. S5a). The peak at 1650 cm^{-1} is assigned to MEA-H^+, while the peaks at 1564 and 1492 cm^{-1} are ascribed to $RNHCOO^-$.[52] The peaks at 1435, 1382, and 1329 cm^{-1} are the signals of $-CH_2$ in MEA-H^+ $RNHCOO^-$,[52] while the peak of HCO_3^- is located at 1217 cm^{-1}.[53] This confirms the presence of HCO_3^- in CO_2-loaded 2 M MEA solution, in line with the ^{13}C NMR analysis. During CO_2 capture by TEA, similar signals for TEA-H^+ (1650 cm^{-1}), $-CH_2$ (1452, 1407, 1358, and 1300 cm^{-1}), and HCO_3^- (1217 cm^{-1}), except those for carbamate, are also observed (Fig. S5b).[52,53]

During the electrolysis of CO_2-loaded amine solutions, the *in situ* ATR-FTIR spectra are recorded at potentials from 0.05 to −1.05 V *vs.* RHE under an Ar atmosphere. The background spectrum was recorded at 0.05 V *vs.* RHE for baseline subtraction. However, the same peaks observed for CO_2-loaded amines appear again even after background deduction when applying a small potential, and the peaks progressively intensify when the electrolysis potential shifts negatively. Such a phenomenon is attributed to the surface plasmonic enhancement effect (Fig. 5a and b).[54] Notably, the characteristic peak for CO starts to show at 1857 and 1919 cm^{-1} for MEA and TEA, respectively, when the potential reaches −0.65 V *vs.* RHE. This confirms the generation of CO adsorbed on the active sites of the CoPc/CB catalyst in different manners. In MEA, the CO is bridge-bound (CO_B), while linearly bound CO (CO_L) is formed in TEA, which highlights the impact of the amine structure on CO generation.[55]

Considering that both carbamate and bicarbonate are present in CO_2-loaded MEA solution, we further investigate the evolution of CO_2 capture and conversion over the CoPc/CB catalyst by density functional theory (DFT) calculations (Fig. 5c). CO_2 capture by MEA solution leads to $RNHCOO^-$ and MEA-H^+ easily, which is an exothermal step ($\Delta E = -0.52$ eV). This indicates that CO_2 is readily converted to $RNHCOO^-$ after

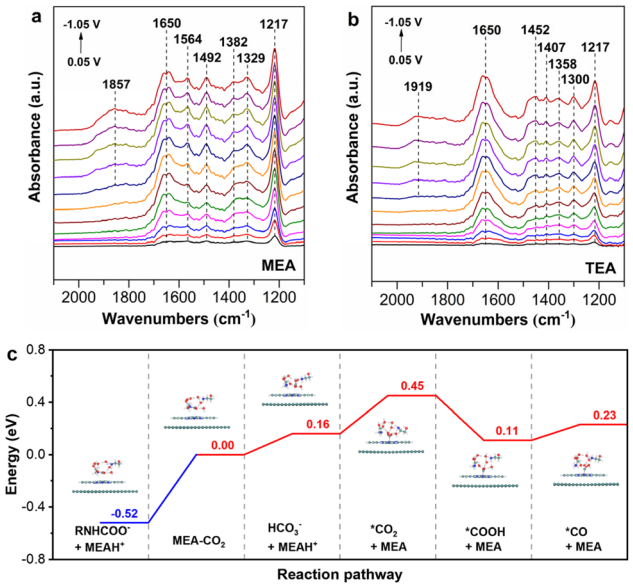

Fig. 5 *In situ* ATR-FTIR spectra recorded for electrolysis of captured CO_2 in 2 M (a) MEA and (b) TEA solutions at different applied potentials using the CoPc/CB catalyst. (c) The energy diagram for the conversion process of captured CO_2 in MEA on the CoPc/CB catalyst. The green, blue, red, and white balls denote C, N, O, and H atoms, respectively.

it is captured by the MEA solution. To explore the reaction process, we examine the pathways of CO_2 transfer: MEA captures CO_2 for direct transfer to the Co active site and CO_2 undergoes HCO_3^- relaying before transferring to the Co site. The direct transfer of CO_2 captured by MEA solution to the Co active site requires an energy of 0.45 eV, while the energy required to convert CO_2 captured by MEA to HCO_3^- is only 0.16 eV. Thus, it is highly favourable for the formation of HCO_3^- in CO_2-loaded MEA solution, which is confirmed by ^{13}C NMR and *in situ* IR spectra. Afterwards, HCO_3^- can dissociate into CO_2 which is adsorbed onto the Co site of the catalyst ($*CO_2$), requiring an energy of 0.29 eV. Previous studies on direct electrolysis of bicarbonate solutions also show that CO_2 originating from HCO_3^- dissociation is the reactant for CO generation.[34,35,56,57] On the other hand, the direct transformation of $RNHCOO^-$ into $*CO_2$ has a much higher energy change of 0.97 V. This explains why the consumption of HCO_3^-, instead of $RNHCOO^-$, is observed in ^{13}C NMR after electrolysis. As long as $*CO_2$ is formed, it is readily activated and converted to *COOH and *CO intermediates on the Co site with an energy requirement of −0.34 and 0.12 eV, respectively.

The distinctions of the HER in MEA and TEA solutions can be attributed to the different properties of the hydrogen source. There are several hydrogen sources that can be reduced to generate H_2 in the two solutions, including H_2O, HCO_3^-, and protonated ammoniums (MEA-H^+/TEA-H^+). The pK_a values for H_2O, HCO_3^-, MEA-H^+, and TEA-H^+ are 14.0, 10.3, 9.4, and 7.8, respectively.[58,59] Thus, MEA-H^+ and TEA-H^+ are more likely the reactants for hydrogen evolution in MEA and TEA solutions, respectively, as they both have lower pK_a values than H_2O and HCO_3^-. This also explains why the HER is more pronounced in

the amine solutions than in the bicarbonate electrolyte.[35,56,59] However, $|j_{H_2}|$ and FE_{H_2} in CO_2-loaded TEA are both lower than in MEA, despite the lower pK_a of TEA-H$^+$. This suggests that the pK_a is not the primary factor determining the efficiency of hydrogen evolution in these amine solutions.

Furthermore, we calculate the adsorption energy (E_{ads}) of MEA-H$^+$ and TEA-H$^+$ on the Co site (Fig. S6). The results show that the E_{ads} of TEA-H$^+$ is −3.56 eV, which is lower than that of MEA-H$^+$ (−3.15 eV). In this sense, TEA-H$^+$ should be more readily adsorbed onto the Co site and thus more favourable for the HER. The energy required for H transferred from MEA-H$^+$ or TEA-H$^+$ to the Co active site is also calculated, which shows a low energy barrier of 0.38 eV for H$^+$ transfer from TEA-H$^+$, while it is 0.66 eV in the case of MEA-H$^+$ (Fig. S7). When the H is transferred onto Co sites, it follows the same pathway for H_2 generation. The calculation results indicate that the HER is more likely to occur for TEA-H$^+$, which is contrary to the electrolysis results. Therefore, neither the E_{ads} nor the energy barrier for H transfer is the key factor determining HER efficiency. There must be another parameter governing the HER process.

Effect of mass transport

The viscosity test shows that CO_2-loaded 2 M TEA solution is more viscous than its MEA and DEA counterparts, which would hinder the mass transport of reactive species in CO_2-loaded TEA solution to a larger extent (Table S3). To verify this hypothesis, we employ ferrocenemethanol as the redox couple to determine the diffusion coefficients of CO_2-loaded 2 M MEA, DEA, and TEA solutions through cyclic voltammetry, which are 3.94, 3.06, and 1.91×10^{-10} m^2 s^{-1}, respectively (Fig. 6a and S8). Notably, CO_2-loaded TEA exhibits the smallest diffusion coefficient, indicating the most hindered mass transport of both HCO_3^- for CO production and TEA-H$^+$ for the HER. This explains the lower $|j_{CO}|$ and $|j_{H_2}|$ observed in TEA than in MEA (Fig. 2b and c).

Given that CO_2-loaded amine solutions contain carbamate/bicarbonate anions along with protonated ammonium cations, it is not clear which ion predominantly determines the diffusion coefficients of these solutions. To disentangle and understand the individual effect of these ions, we conduct additional cyclic voltammetry tests in ammonium chloride solutions of the corresponding amines. These solutions share the same anions (Cl^-) but differ only in the ammonium cations. Their diffusion coefficients follow the same sequence of MEA-H$^+$Cl$^-$ (4.36×10^{-10} m^2 s^{-1}) > DEA-H$^+$Cl$^-$ (3.44×10^{-10} m^2 s^{-1}) > TEA-H$^+$Cl$^-$ (2.29×10^{-10} m^2 s^{-1}) (Fig. 6b and S8). Notably, the diffusion coefficient of MEA-H$^+$Cl$^-$ is nearly twice that of TEA-H$^+$Cl$^-$. Additionally, we measure the diffusion coefficient of 2 M $KHCO_3$, which shares the same bicarbonate anion with CO_2-loaded 2 M TEA but differs in the cations. The diffusion coefficient of 2 M $KHCO_3$ is 6.02×10^{-10} m^2 s^{-1}, which is more than three times larger than that of CO_2-loaded 2 M TEA. This demonstrates that the ammonium cations significantly influence the mass transport, with the larger TEA-H$^+$ cation imposing a greater hindrance to the diffusion of solution components.

We further compared the diffusion coefficients of CO_2-loaded amine solutions with those of their corresponding ammonium chloride solutions, which share the same ammonium cations but differ in anions (carbamate/bicarbonate *vs.* Cl^-). In all cases, the CO_2-loaded amine solutions exhibit slightly smaller diffusion coefficients, suggesting that the change of carbamate/bicarbonate to Cl^- has only a minor effect on the mass transport.

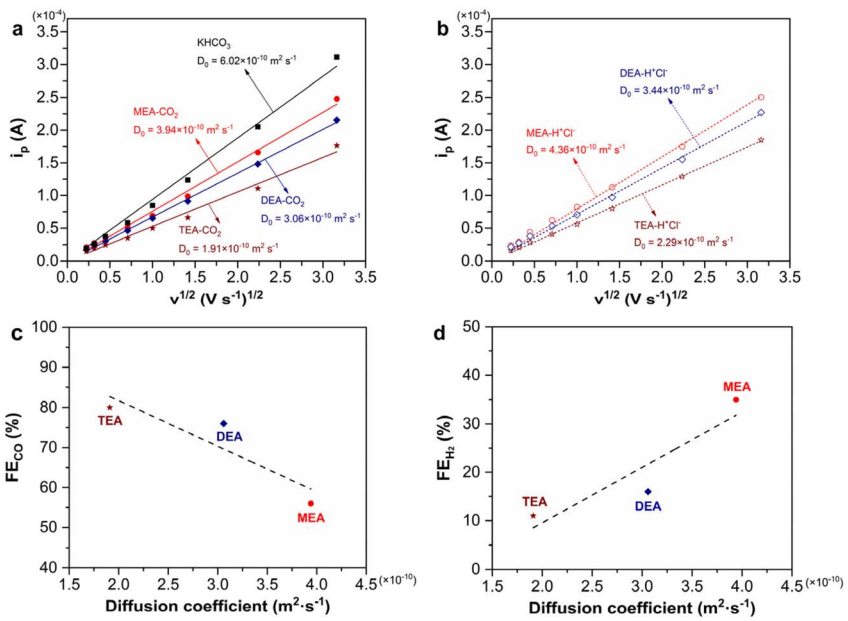

Fig. 6 Plot of the peak currents for ferrocenemethanol oxidation (i_p) *versus* the square root of scan rates from cyclic voltammetry tests of (a) CO_2-loaded 2 M amine solutions, 2 M $KHCO_3$, and (b) ammonium chloride solutions of the corresponding amines. The correlation of (c) FE_{CO} and (d) FE_{H_2} for electrolysis of CO_2-loaded 2 M amine solutions at −0.85 V *vs.* RHE with the diffusion coefficients of the solutions.

The comparison of diffusion coefficients clearly reveals that the mass transport of TEA-H^+ is more significantly hindered in CO_2-loaded TEA solution, whereas the HCO_3^- transport is less affected. This restriction severely suppresses the competing HER, resulting in the highest CO selectivity in TEA. Indeed, there is a negative correlation between FE_{CO} for the electrolysis of captured CO_2 and the diffusion coefficients of CO_2-loaded amine solutions, while a positive correlation between FE_{H_2} and the diffusion coefficients is observed (Fig. 6c and d).

Therefore, while there is a shift in the $RNHCOO^- \rightleftharpoons HCO_3^-$ equilibrium (eqn (5)) in CO_2-loaded MEA solution during electrolysis, such a shift is expected to have little effect on the mass transport limitation caused by the large ammonium cations. This is because such a shift only alters the relative distribution of anionic species ($RNHCOO^-$ *vs.* HCO_3^-) without changing cations in MEA solution. In contrast, TEA solution does not exhibit this equilibrium shift, containing only HCO_3^- anions and THE-H^+ cations (eqn (6)). Over extended operation for electrolysis, both HCO_3^- and TEA-H^+ will be consumed for CO production, while TEA will be regenerated. Since TEA is also a large molecule, the mass transport limitation persists in TEA solution.

The effect of mass transport is further verified by conducting the electrolysis of captured CO_2 in 2 M MEA solution using D_2O as the solvent (Fig. S9). It is known that the self-diffusion coefficient of D_2O is 1.87×10^{-9} m^2 s^{-1}, lower than that of H_2O (2.35×10^{-9} m^2 s^{-1}).[60] Thus, using D_2O as the solvent can reduce the transport rate of MEA-H^+ in MEA solution. As expected, the FE_{CO} is enhanced while the HER is remarkably inhibited when using D_2O as the solvent. More importantly, the decrease in FE_{CO} and the increase in FE_{H_2} also slow down after replacing H_2O with D_2O, showing better stability in D_2O. These results unequivocally confirm that the mass transport of MEA-H^+ and TEA-H^+ in the electrolyte plays a crucial role in the HER, and affects the selectivity for CO production and the stability of the catalyst.

To investigate whether this mass transport mechanism applies to other common catalysts, we performed electrolysis of captured CO_2 in 2 M MEA and TEA solutions using Ni–N–C or Ag nanopowder as the catalyst. Ni–N–C achieved high FE_{CO} (>90%) for electrochemical CO_2 conversion at low current densities in an H-cell and high current densities in a flow cell,[38] and showed much better stability than CoPc/CB for electrochemical conversion of bicarbonate solution, which is a common captured CO_2 coming from hydroxide and carbonate solutions.[56] It can be seen from Fig. S10 that Ni–N–C consistently exhibits higher FE_{CO} and lower FE_{H_2} in TEA than in MEA across all electrolysis potentials, revealing the same trend as that using CoPc/CB. This suggests that the mass transport effect also applies to the Ni–N–C catalyst for electrochemical conversion of CO_2-loaded amine solutions. To our surprise, Ni–N–C exhibits lower CO selectivity and poorer stability than CoPc/CB in TEA (Fig. S10 and S11). Since Ni–N–C exhibits higher stability for the conversion of both CO_2 and bicarbonate solution, we propose that the poorer performance for Ni–N–C originates from the effect of the CO_2-loaded amine environment rather than from the catalyst itself, which warrants a systematic study.

In contrast to CoPc/CB and Ni–N–C, the Ag catalyst exhibits higher FE_{CO} in MEA than in TEA across all electrolysis potentials, though FE_{CO} is usually lower than FE_{H_2} for both solutions (Fig. S12). This difference likely stems from the distinct structure of the Ag catalyst (nanopowder) compared to CoPc/CB and Ni–N–C catalysts with highly dispersed metal sites. This structure difference leads to different adsorption behaviours of reactive species (*e.g.*, protonated ammonium, carbamate, and bicarbonate) on nanostructured Ag sites *versus* isolated Co sites in CoPc/CB or isolated Ni sites dispersed in Ni–N–C. These results demonstrate that the mass transport mechanism applies to isolated metal sites, including supported metal complexes and single atom catalysts, two common types of CO_2 conversion catalysts, but does not hold for nanostructured Ag catalysts.

Based on all the experimental results, we propose the reaction mechanism for electrochemical conversion of captured CO_2 in various amine solutions (Fig. 7). For primary and secondary amines such as MEA and DEA, the carbamate species is first formed after CO_2 capture and then transformed into the bicarbonate species partially. For tertiary amines such as TEA, it captures CO_2 to form bicarbonate directly. When a reduction potential is applied, the bicarbonate dissociates into CO_2, which is adsorbed onto the active site of the CoPc/CB catalyst and gets reduced to form the CO product. Concurrently, hydrogen evolution occurs through the reduction of protonated amines, which compete with CO production. Due to the restrained mass transport of TEA-H^+, the HER is significantly suppressed in CO_2-loaded TEA solution, resulting in higher CO selectivity and stability for electrolysis.

It has to be pointed out that the direct electrochemical conversion of captured CO_2 in amine solutions becomes more complicated when it goes to application-relevant configurations, such as membrane electrode assemblies. Our previous study on the direct electrolysis of $KHCO_3$ solution reveals that the real reactant for CO production is CO_2 in both an H-cell and membrane electrode assembly, but the sources of CO_2 are different.[57] In the H-cell, the CO_2 for CO formation primarily comes from the dissociation equilibrium of HCO_3^-, while in

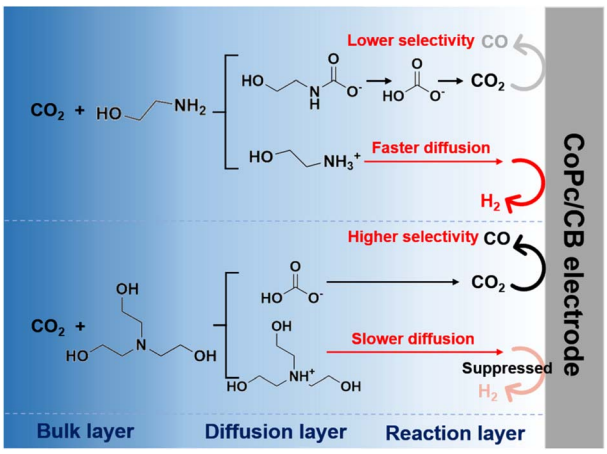

Fig. 7 Proposed reaction mechanism for electrochemical conversion of captured CO_2 in various amine solutions.

membrane electrode assembly a large quantity of CO_2 can be *in situ* generated near the catalyst layer from the reaction between HCO_3^- and H^+ (generated from water splitting on the bipolar membrane), enabling CO production at large current densities. Meanwhile, the H^+ generated near the catalyst layer may also be reduced to yield H_2, competing with CO_2 reduction (CO formation). Such a difference leads to a significant discrepancy of the reactant and reaction process in membrane electrode assembly.

Conclusions

In summary, we have conducted a comprehensive investigation of direct electrochemical conversion of captured CO_2 in primary, secondary, and tertiary amine solutions (MEA, DEA, and TEA) using a CoPc/CB catalyst. Among all amine solutions, the tertiary amine (TEA) exhibits the highest selectivity and stability for the electrochemical conversion of captured CO_2 to CO. Experimental evidence and DFT calculations collectively identify bicarbonate-derived CO_2, rather than carbamate, as the real reactive species for CO production regardless of amine types. More crucially, we demonstrate that mass transport governs both the electrochemical conversion of captured CO_2 and the competing reduction of protonated ammonium. In TEA, the transport of both bicarbonate and TEA-H^+ is hindered, with the greater hindrance to TEA-H^+ diffusion suppressing hydrogen evolution more significantly. This accounts for the high selectivity and stability for CO production observed in TEA. These findings provide fundamental insights into the reaction pathway of electrochemical conversion of captured CO_2 and establish mass transport manipulation as a key strategy for accomplishing high conversion efficiency.

Direct electrochemical conversion of captured CO_2 in amine solutions shows great promise, as it bypasses conventional steps such as CO_2 release, purification, and compression, resulting in significant energy savings. However, the long-term electrolysis stability of CO_2-loaded amine solutions remains insufficient, primarily due to intensified competing hydrogen evolution. Therefore, future efforts should focus on suppressing the hydrogen evolution reaction—for example, by modifying the working electrode with positive charges to repel the approaching of protonated ammonium ions—thereby improving the selectivity and long-term stability of electrolysis at industrially relevant current densities. Meanwhile, the design and engineering of electrolyzers (*e.g.*, membrane electrode assemblies) tailored for industrial applications at reduced cell voltages is also crucial to further lower energy consumption, thereby constructing an energy-efficient and durable system for direct electrolysis of captured CO_2 in amine solutions.

Author contributions

Z. L. conducted the study, prepared the catalyst, performed electrolysis, NMR analyses, and *in situ* ATR-FTIR, and wrote the manuscript. K. L. conducted the DFT calculations and wrote the manuscript. C.-Q. Y. and L. D. contributed to the preparation of the manuscript. M. L. and X.-M. H. revised the manuscript, provided the funding support, and supervised the work.

Conflicts of interest

The authors declare no competing financial interest.

Data availability

All data needed to evaluate the conclusions are present in the paper and the supplementary information (SI). Supplementary information is available. See DOI: https://doi.org/10.1039/d6sc00859c.

Acknowledgements

This work was financially supported by the National Natural Science Foundation of China (22376120 and 22376222), the Taishan Scholars program from Shandong Province (tsqn202103021), the Science and Technology lnnovation Program of Hunan Province (2023RC1012), and the Central South University Research Program of Advanced Interdisciplinary Studies (2023QYJC012).

Notes and references

1 R. D. Bressler, The mortality cost of carbon, *Nat. Commun.*, 2021, **12**, 4467.
2 T. Geng, F. Jia, W. Cai, L. Wu, B. Gan, Z. Jing, S. Li and M. J. McPhaden, Increased occurrences of consecutive La Niña events under global warming, *Nature*, 2023, **619**, 774–781.
3 X. She, Y. Wang, H. Xu, S. Chi Edman Tsang and S. Ping Lau, Challenges and opportunities in electrocatalytic CO_2 reduction to chemicals and fuels, *Angew. Chem., Int. Ed.*, 2022, **61**, e202211396.
4 T. Yan, X. Chen, L. Kumari, J. Lin, M. Li, Q. Fan, H. Chi, T. J. Meyer, S. Zhang and X. Ma, Multiscale CO_2 electrocatalysis to C_{2+} products: reaction mechanisms, catalyst design, and device fabrication, *Chem. Rev.*, 2023, **123**, 10530–10583.
5 M. Jiang, H. Wang, M. Zhu, X. Luo, Y. He, M. Wang, C. Wu, L. Zhang, X. Li, X. Liao, Z. Jiang and Z. Jin, Review on strategies for improving the added value and expanding the scope of CO_2 electroreduction products, *Chem. Soc. Rev.*, 2024, **53**, 5149–5189.
6 U. Nzotcha, S. Sanz, H. Tempel and R. A. Eichel, Technoeconomic perspective on the electroreduction of CO_2 to formic acid: scale-up strategies toward industrial viability, *Angew. Chem., Int. Ed.*, 2025, **64**, e202418114.
7 D. U. Nielsen, X.-M. Hu, K. Daasbjerg and T. Skrydstrup, Chemically and electrochemically catalysed conversion of CO_2 to CO with follow-up utilization to value-added chemicals, *Nat. Catal.*, 2018, **1**, 244–254.
8 Y. Hu, C. C. Lee, M. Grosch, J. B. Solomon, W. Weigand and M. W. Ribbe, Enzymatic Fischer–Tropsch-type reactions, *Chem. Rev.*, 2022, **123**, 5755–5797.

9 W. Wu and Y. Wang, The role of protons in CO_2 reduction on gold under acidic conditions, *J. Am. Chem. Soc.*, 2025, **147**, 11662–11666.
10 F. Nkurunziza, S. Dongare, S. Chatterjee, B. Shah, M. Gautam, B. Muchharla, B. Kumar, M. J. Janik, B. Gurkan, R. L. Sacci and J. M. Spurgeon, Alkali cation inhibition of imidazolium-mediated electrochemical CO_2 reduction on silver, *J. Am. Chem. Soc.*, 2025, **147**, 7564–7577.
11 X. Zhang, Y. Wang, M. Gu, M. Wang, Z. Zhang, W. Pan, Z. Jiang, H. Zheng, M. Lucero, H. Wang, G. E. Sterbinsky, Q. Ma, Y. G. Wang, Z. Feng, J. Li, H. Dai and Y. Liang, Molecular engineering of dispersed nickel phthalocyanines on carbon nanotubes for selective CO_2 reduction, *Nat. Energy*, 2020, **5**, 684–692.
12 W. Liu, P. Bai, S. Wei, C. Yang and L. Xu, Gadolinium changes the local electron densities of nickel 3d orbitals for efficient electrocatalytic CO_2 reduction, *Angew. Chem., Int. Ed.*, 2022, **61**, e202201166.
13 M. Fang, L. Xu, H. Zhang, Y. Zhu and W. Y. Wong, Metalloporphyrin-linked mercurated graphynes for ultrastable CO_2 electroreduction to CO with nearly 100% selectivity at a current density of 1.2 A cm^{-2}, *J. Am. Chem. Soc.*, 2022, **144**, 15143–15154.
14 P. Hutchison, L. E. Smith, C. L. Rooney, H. Wang and S. Hammes Schiffer, Proton-coupled electron transfer mechanisms for CO_2 reduction to methanol catalyzed by surface-immobilized cobalt phthalocyanine, *J. Am. Chem. Soc.*, 2024, **146**, 20230–20240.
15 Q. Wang, K. Liu, J. Fu, C. Cai, H. Li, Y. Long, S. Chen, B. Liu, H. Li, W. Li, X. Qiu, N. Zhang, J. Hu, H. Pan and M. Liu, Atomically eispersed s-block magnesium sites for electroreduction of CO_2 to CO, *Angew. Chem., Int. Ed.*, 2021, **60**, 25241–25245.
16 S. Li, S. Zhao, X. Lu, M. Ceccato, X.-M. Hu, A. Roldan, J. Catalano, M. Liu, T. Skrydstrup and K. Daasbjerg, Low-valence $Zn^{\delta+}$ ($0<\delta<2$) single-atom material as highly efficient electrocatalyst for CO_2 reduction, *Angew. Chem., Int. Ed.*, 2021, **60**, 22826–22832.
17 Y. Li, N. M. Adli, W. Shan, M. Wang, M. J. Zachman, S. Hwang, H. Tabassum, S. Karakalos, Z. Feng, G. Wang, Y. C. Li and G. Wu, Atomically dispersed single Ni site catalysts for high-efficiency CO_2 electroreduction at industrial-level current densities, *Energy Environ. Sci.*, 2022, **15**, 2108–2119.
18 T. Liu, T. Xu, T. Li and Y. Jing, Selective CO_2 reduction over γ-graphyne supported single-atom catalysts: crucial role of strain regulation, *J. Am. Chem. Soc.*, 2024, **146**, 24133–24140.
19 A. M. Zito, L. E. Clarke, J. M. Barlow, D. Bím, Z. Zhang, K. M. Ripley, C. J. Li, A. Kummeth, M. E. Leonard, A. N. Alexandrova, F. R. Brushett and J. Y. Yang, Electrochemical carbon dioxide capture and concentration, *Chem. Rev.*, 2023, **123**, 8069–8098.
20 Q. Xia, K. Zhang, T. Zheng, L. An, C. Xia and X. Zhang, Integration of CO_2 capture and electrochemical conversion, *ACS Energy Lett.*, 2023, **8**, 2840–2857.
21 T. Zheng, K. Jiang, N. Ta, Y. Hu, J. Zeng, J. Liu and H. Wang, Large-scale and highly selective CO_2 electrocatalytic reduction on nickel single-atom catalyst, *Joule*, 2019, **3**, 265–278.
22 Z. Qi, A. R. Kashi, A. K. Buckley, J. S. Miller, J. Ye, M. M. Biener, A. C. Foucher, E. A. Stach, S. Ma, K. P. Kuhl and J. Biener, Effect of gold catalyst surface morphology on wetting behavior and eectrochemical CO_2 reduction performance in a large-area zero-gap gas diffusion electrolyzer, *J. Phys. Chem. C*, 2022, **126**, 19637–19646.
23 J. A. Rabinowitz and M. W. Kanan, The future of low-temperature carbon dioxide electrolysis depends on solving one basic problem, *Nat. Commun.*, 2020, **11**, 5231.
24 I. Sullivan, A. Goryachev, I. A. Digdaya, X. Li, H. A. Atwater, D. A. Vermaas and C. Xiang, Coupling electrochemical CO_2 conversion with CO_2 capture, *Nat. Catal.*, 2021, **4**, 952–958.
25 M. Li, E. Irtem, H.-P. Iglesias van Montfort, M. Abdinejad and T. Burdyny, Energy comparison of sequential and integrated CO_2 capture and electrochemical conversion, *Nat. Commun.*, 2022, **13**, 5398.
26 K. Shen, D. Cheng, E. Reyes-Lopez, J. Jang, P. Sautet and C. G. Morales-Guio, On the origin of carbon sources in the electrochemical upgrade of CO_2 from carbon capture solutions, *Joule*, 2023, **7**, 1260–1276.
27 G. Lee, A. S. Rasouli, B.-H. Lee, J. Zhang, D. H. Won, Y. C. Xiao, J. P. Edwards, M. G. Lee, E. D. Jung, F. Arabyarmohammadi, H. Liu, I. Grigioni, J. Abed, T. Alkayyali, S. Liu, K. Xie, R. K. Miao, S. Park, R. Dorakhan, Y. Zhao, C. P. O'Brien, Z. Chen, D. Sinton and E. Sargent, CO_2 electroreduction to multicarbon products from carbonate capture liquid, *Joule*, 2023, **7**, 1277–1288.
28 M. C. Freyman, Z. Huang, D. Ravikumar, E. B. Duoss, Y. Li, S. E. Baker, S. H. Pang and J. A. Schaidle, Reactive CO_2 capture: a path forward for process integration in carbon management, *Joule*, 2023, **7**, 631–651.
29 H. Song, C. A. Fernández, H. Choi, P.-W. Huang, J. Oh and M. C. Hatzell, Integrated carbon capture and CO production from bicarbonates through bipolar membrane electrolysis, *Energy Environ. Sci.*, 2024, **17**, 3570–3579.
30 X.-M. Hu, H.-Q. Liang, A. Rosas Hernández and K. Daasbjerg, Electrochemical valorization of captured CO_2: recent advances and future perspectives, *Chem. Soc. Rev.*, 2025, **54**, 1216–1250.
31 M. Biermann, F. Normann, F. Johnsson, R. Hoballah and K. Onarheim, Capture of CO_2 from steam reformer flue gases using monoethanolamine: pilot plant validation and process design for partial capture, *Ind. Eng. Chem. Res.*, 2022, **61**, 14305–14323.
32 K. Jiang, H. Yu, Z. Sun, Z. Lei, K. Li and L. Wang, Zero-emission cement plants with advanced amine-based CO_2 capture, *Environ. Sci. Technol.*, 2024, **58**, 6978–6987.
33 G. Lee, Y. C. Li, J.-Y. Kim, T. Peng, D.-H. Nam, A. Sedighian Rasouli, F. Li, M. Luo, A. H. Ip, Y.-C. Joo and E. H. Sargent, Electrochemical upgrade of CO_2 from amine capture solution, *Nat. Energy*, 2020, **6**, 46–53.
34 G. Leverick, E. M. Bernhardt, A. I. Ismail, J. H. Law, A. Arifutzzaman, M. K. Aroua and B. M. Gallant,

Uncovering the active species in amine-mediated CO_2 reduction to CO on Ag, *ACS Catal.*, 2023, **13**, 12322–12337.
35 J. H. Kim, H. Jang, G. Bak, W. Choi, H. Yun, E. Lee, D. Kim, J. Kim, S. Y. Lee and Y. J. Hwang, The insensitive cation effect on a single atom Ni catalyst allows selective electrochemical conversion of captured CO_2 in universal media, *Energy Environ. Sci.*, 2022, **15**, 4301–4312.
36 P. Li, Y. Mao, H. Shin, Q. Yang, X. Cheng, Y. Li, K. Li, H. Yu, R. Mulder, W. K. Pang, H. Jin, Y. Zhao, Z. Zheng, E. Finch, K. Hearn, B. Jia, G. I. N. Waterhouse, Z. Wang and T. Ma, Tandem amine scrubbing and CO_2 electrolysis via direct piperazine carbamate reduction, *Nat. Energy*, 2025, **10**, 1262–1273.
37 Y.-J. Kong, Y.-B. Zou, T.-W. Jiang, K. Jiang and X.-M. Hu, Closed-loop synthesis of highly dispersed cobalt phthalocyanine catalysts for efficient CO_2 electroreduction, *ACS Sustainable Resour. Manage.*, 2024, **1**, 778–786.
38 L.-H. Feng, Z.-H. Lv, Y.-J. Kong and X.-M. Hu, Upcycling of plastic waste to atomic nickel site-decorated carbon for efficient electrochemical CO_2 conversion, *Sustain. Energy Fuels*, 2024, **8**, 2860–2868.
39 N. Elgrishi, K. J. Rountree, B. D. McCarthy, E. S. Rountree, T. T. Eisenhart and J. L. Dempsey, A practical beginner's guide to cyclic voltammetry, *J. Chem. Educ.*, 2017, **95**, 197–206.
40 G. Kresse and J. Furthmuller, Efficient iterative schemes for ab initio total-energy calculations using a plane-wave basis set, *Phys. Rev. B: Condens. Matter Mater. Phys.*, 1996, **54**, 11169–11186.
41 G. Kresse and J. Furthmuller, Efficiency of ab-initio total energy calculations for metals and semiconductors using a plane-wave basis set, *Comput. Mater. Sci.*, 1996, **6**, 15–50.
42 P. E. Blöchl, Projector augmented-wave method, *Phys. Rev. B: Condens. Matter Mater. Phys.*, 1994, **50**, 17953–17979.
43 J. P. Perdew, J. A. Chevary, S. H. Vosko, K. A. Jackson, M. R. Pederson, D. J. Singh and C. Fiolhais, Atoms, molecules, solids, and surfaces: applications of the generalized gradient approximation for exchange and correlation, *Phys. Rev. B: Condens. Matter Mater. Phys.*, 1992, **46**, 6671–6687.
44 J. P. Perdew, K. Burke and M. Ernzerhof, Generalized gradient approximation made simple, *Phys. Rev. Lett.*, 1996, **77**, 3865–3868.
45 S. Grimme, Semiempirical GGA-type density functional constructed with a long-range dispersion correction, *J. Comput. Chem.*, 2006, **27**, 1787–1799.
46 K. Mathew, R. Sundararaman, K. Letchworth Weaver, T. A. Arias and R. G. Hennig, Implicit solvation model for density-functional study of nanocrystal surfaces and reaction pathways, *J. Chem. Phys.*, 2014, **140**, 084106.
47 K. Mathew, V. S. C. Kolluru, S. Mula, S. N. Steinmann and R. G. Hennig, Implicit self-consistent electrolyte model in plane-wave density-functional theory, *J. Chem. Phys.*, 2019, **151**, 234101.
48 A. Q. Mir, A. Banerjee, F. Ihiri, S. Chiu, A. N. Alexandrova, C. Morales-Guio and J. Y. Yang, Optimizing CO_2-Loaded Aqueous Amine Solutions for Higher Electrocatalytic CO_2 Reduction Activity, *J. Am. Chem. Soc.*, 2025, **147**, 39123–39133.
49 J. Jiang, A. J. Matula, J. R. Swierk, N. Romano, Y. Wu, V. S. Batista, R. H. Crabtree, J. S. Lindsey, H. Wang and G. W. Brudvig, Unusual stability of a bacteriochlorin electrocatalyst under reductive conditions. a case study on CO_2 conversion to CO, *ACS Catal.*, 2018, **8**, 10131–10136.
50 A. García Abuín, D. Gómez Díaz, A. B. López, J. M. Navaza and A. Rumbo, NMR characterization of carbon dioxide chemical absorption with monoethanolamine, diethanolamine, and triethanolamine, *Ind. Eng. Chem. Res.*, 2013, **52**, 13432–13438.
51 B. Lv, B. Guo, Z. Zhou and G. Jing, Mechanisms of CO_2 capture into monoethanolamine solution with different CO_2 loading during the absorption/desorption processes, *Environ. Sci. Technol.*, 2015, **49**, 10728–10735.
52 D. F. Bruggeman, G. Rothenberg and A. C. Garcia, Investigating proton shuttling and electrochemical mechanisms of amines in integrated CO_2 capture and utilization, *Nat. Commun.*, 2024, **15**, 9207.
53 K. Coenen, F. Gallucci, B. Mezari, E. Hensen and M. van Sint Annaland, An in-situ IR study on the adsorption of CO_2 and H_2O on hydrotalcites, *J. CO2 Util.*, 2018, **24**, 228–239.
54 Z. Lin, N. Blake, X. Pang, Z. He, G. Mirshekari, O. Romiluyi, Y. J. Son, S. Kabra and D. V. Esposito, Oxide-encapsulated silver electrocatalysts for selective and stable syngas production from reactive carbon capture solutions, *Angew. Chem., Int. Ed.*, 2024, **63**, e202404758.
55 M. Dunwell, Y. Yan and B. Xu, In situ infrared spectroscopic investigations of pyridine-mediated CO_2 reduction on Pt electrocatalysts, *ACS Catal.*, 2017, **7**, 5410–5419.
56 Y.-B. Zou, A.-C. Zheng, L.-H. Feng, L. Du, K. Daasbjerg and X.-M. Hu, Integrated capture and electrochemical conversion of CO_2 from flue gas mediated by carbonate/bicarbonate cycle, *J. Mater. Chem. A*, 2025, **13**, 36191–36201.
57 L.-H. Feng, N. Wang, Y.-B. Zou, Y. Li and X.-M. Hu, Dissecting key factors influencing electrochemical conversion of carbon solutions over nickel single atoms, *Small*, 2025, **21**, 2410719.
58 J. H. Kim, C. Dobrogowska and L. G. Hepler, Thermodynamics of ionization of aqueous alkanolamines, *Can. J. Chem. Eng.*, 1987, **65**, 1726.
59 J. Safipour, A. Z. Weber and A. T. Bell, Detrimental effects of monoethanolamine and other amine-based capture agents on the electrochemical reduction of CO_2, *ACS Energy Lett.*, 2023, **8**, 5012–5017.
60 H.-Q. Liang, S. Zhao, X.-M. Hu, M. Ceccato, T. Skrydstrup and K. Daasbjerg, Hydrophobic copper interfaces boost electroreduction of carbon dioxide to ethylene in water, *ACS Catal.*, 2021, **11**, 958–966.